Turbulent dissipation on the margins of the South China Sea

Louis St. Laurent
Department of Oceanography
Florida State University
Tallahassee, FL, USA
lous@ocean.fsu.edu

Accepted for publication in Geophysical Research Letters
10 October 2008

Abstract

Measurements of turbulence along the continental slope, shelfbreak, and shelf of the northern South China Sea are presented from a 10-day measurement program during April 2005. The shelfbreak region was characterized by a deep stratification that appears to be typical of the late winter-monsoon. This appears to shift the wave field at the shelfbreak from the soliton-like depression anomalies observed in previous years to a more complex wave field, supporting high-frequency waves in both upper and lower depth-intervals of the water column. On average, 30% of the depth-integrated turbulent dissipation occurs within 10 m of the bottom, where baroclinic energy is preferentially dissipated. Dissipation levels, reaching 50 mW/m^2, are an order of magnitude larger than those attainable through frictional dissipation of the local barotropic tide, and an order of magnitude larger than levels typical in the open ocean.

Introduction

Large amplitude internal waves are a long recognized feature of the South China Sea (SCS). Remote sensing imagery often shows the sea-surface manifestation of these waves as they radiate from the Luzon Passage into the deep water of the South China Sea [*Hsu et al., 2000*]. *In situ* observations have shown that the waves occur as soliton-like coherent packets, creating depressions in the thermocline stratification with wavelengths of O(1 km). These waves are described as nonlinear, with their steepness often exceeding a slope of 1/50. In the deep basin west of Luzon, the waves have typical displacement amplitudes exceeding 100 m, and persist for several days as they propagate toward China and Vietnam. The waves reach the shallow continental shelf along China after 2-3 days, where the packets become stretched into longer trains of waves.

The nonlinear waves of the SCS were previously studied during the Asian Seas International Acoustics Experiment (ASIAEX), primarily during May 2001. Time-series measurements of the waves are described in several papers [e.g., *Duda et al*., 2004; *Yang et al.*, 2004]. Process-oriented observations of shoaling waves were made by *Orr and Mignerey* [2003], who used high-frequency acoustic imagery to reveal details of wave evolution along the continental slope. Their imagery showed the conversion of depression waves into elevation waves occurring near the 200-m isobath. Specific wave packets were tracked by ship, and simultaneous Acoustic Doppler Current Profiler (ADCP) velocity measurements were used to estimate wave energy. *Orr and Mignerey* [2003] reported significant energy exchange between individual crests as the wave groups spread over larger horizontal length scales. They also observed instabilities in the form of wave overturns.

Additional work during ASIAEX included moored ADCP measurements [*Lien et al.,* 2005; *Chang et al.*, 2006). These data were interpreted to show a strong divergence of kinetic energy as the Luzon waves shoal, presumably due to dissipation. *Lien et al.* [2005] find that the shelfbreak region of the northern SCS typically exhibits four-times the baroclinic energy of the typical, mid-latitude open ocean. Based on these previous studies, it is reasonable to expect that the SCS has one of the most dissipative margins in the global ocean. Here, we present what we believe are the first measurements of turbulent dissipation observations from this region.

Measurements

During April 2005, we participated in a 10-day field survey on the continental slope and shelf of the SCS on the Taiwanese vessel *Ocean Researcher I (R/V OR1)*. This study was done in conjunction with groups from National Taiwan University, Woods Hole Oceanographic Institution, and Naval Postgraduate School. The Florida State University group used a Sea and Sun Technology *MSS* vertical turbulence profiler [*Wolk et al.*, 2004]. This profiling system was operated using a slack tether spooled from a rail-mounted winch, allowing for a free-fall descent. Sensors on the profiler included a standard CTD, as well as dual airfoil probes from the measurement of microstructure shear, and an FP07 fast thermistor for the measurement of microstructure temperature. Here, we will focus on the micro-shear measurements and the resulting estimates of turbulent kinetic energy dissipation rate: $\varepsilon = (15/2)\nu\overline{u_z^2}$, where ν is the molecular viscosity and $\overline{u_z^2}$ is mean-square micro-shear. Estimates of ε were made in 1-m vertical bins based on spectral analysis of the shear signal from the two probes [*Gregg*, 1999]. The noise level of the dissipation estimates is $\varepsilon \approx 1\times10^{-9}$ W/kg, due to instrument vibrations contaminating the shear probe signals.

The field survey began on April 11, during spring tide conditions and continued through neap tide conditions on April 20. This survey included spatial survey work between the 40-m and the 320-m isobaths, a 12-hr occupation of the 160-m isobath, and time-series measurements at several other sites that will not be described here. Figure 1 shows the bathymetry contours of the region, indicating the steep continental slope between the deep basin of the SCS and the continental shelf. In total, 348 full-depth MSS profiles were collected between the 40-m and 320-m isobaths during the survey. One particular survey was done on April 19 during a 16-hour north to south transect at roughly 117.3°E. The station locations sampled during this synoptic survey are shown in Figure 1. The orientation of this transect roughly follows the refractive path of the waves. Temperature contours from this section are shown in Figure 2. The isotherm structure clearly indicates the presence of a slope current, seaward of the 100-m isobath, as described by *Gawarkiewicz et al.*, [2004].

All 348 dissipation rate profiles made throughout the 10-day survey were generally reoccupations of the same station locations shown in Figure 1. Dissipation estimates were sorted into 10 0.1-latitude bins, and averaged in each bin to produce statistically stable means over the length of the survey region. These 10 average profiles are also shown in Figure 2. This section indicates that the most intense turbulence levels occur in the shelfbreak region, with column integrated dissipation levels $\int_{-H}^{0} \rho\varepsilon\, dz$ exceeding 50 mW/m^2 between the 100-m and 200-m isobaths, in contrast to 10 mW/m^2 levels sea-ward and shore-ward of this region. Along the shelfbreak region, near-bottom dissipation accounts for about 30% of the total depth integrated dissipation. The overall section average is 25 mW/m^2, which is an order of magnitude larger than the average open-ocean dissipation rate for tidal energy [*Munk and Wunsch*, 1998]. Taken with estimates of the buoyancy frequency (N), diffusivity estimates given by $k_\rho = 0.2\ \bar{\varepsilon}/N^2$ [*Osborn*, 1980] along the shelfbreak region exceed 1 cm^2/s, also an order of magnitude above open-ocean

values. For reference, an average buoyancy gradient profile for the shelfbreak region is shown in the inset of Figure 2.

Given the apparent significance of the dissipation processes occurring at the shelfbreak region, it is appropriate to examine the interaction of currents, waves, and turbulence at this site. One 12-hr period was devoted to repeated measurements along the 160-m mean isobath at 21.93°N, 117.35°E during 15 April 2005 from 1130 to 2330 UTC. In total, 80 full-depth profiles were collected.

Acoustic backscatter data were collected during the profiling activity, and the 120 kHz record is shown in Figure 3a. The acoustic imagery clearly indicates that high-frequency wave activity was occurring through the sample period. A strong scattering layer is persistent between 30 m and 100-m depth. This layer seems to deepen in the late portion of the record. Wave activity is not limited to this layer, as numerous events seem to extend all the way to the bottom. The most noteworthy feature of the backscatter record is the bottom anomaly between 1200-1300 UTC. During this period, the ship drifted slightly to the northeast of the 160-m isobath, apparently passing near an abrupt bottom feature. Strong fluctuations of temperature and turbulence accompany this feature (Figure 3b), with elevated turbulence apparently occurring in the wake of the topography. After drifting approximately 1 km (during the gap in the profiler record), the ship repositioned to the original site for continued sampling at the 160-m isobath. After this initial drift, the ship held position to within a 300-m radius.

Turbulence dissipation levels (Fig. 3b) are concentrated near the boundaries, particularly along the bottom, where the largest values of ε were observed. Vertically integrated dissipation levels (Fig 3c), $\int_{-H}^{0} \rho\varepsilon \, dz$, varied between 10 and 50 mW/m^2 during the 12-hr period. The largest integrated levels correspond to particularly strong bottom boundary-layer turbulence. The largest turbulence levels come during the latter half of the record, during the period of the strongest isotherm displacements.

A general comparison between the temperature and backscatter time series shows strong correlation. The temperature contours (Fig 3b) show depth fluctuations of roughly 20 m on the 10-minute sampling timescale for successive profiles. This corresponds to the buoyancy period at 100-m depth (N=5 cyc/hr), but is roughly twice the buoyancy period at 40-m depth (N=10 cyc/hr). Thus, the isotherm displacement record is a low-pass representation of the vertical motions represented in the backscatter imagery.

Using the temperature field observations, we have derived a depth record for isotherms shown in Figure 3b. These depth records were used to calculate displacement relative to the time series mean-depth of each isotherm. The displacement record, $\eta(t)$, was used for the calculation of vertical velocity, $w = d\eta/dt$. A 150 kHz shipboard ADCP system (RD Instruments) was operated to measure horizontal velocity components u and v. These data were processed and averaged to 3-minute bins (Fig. 4). Data from the 20-m surface layer, and the 30-m bottom layer, were discarded due to poor signal-to-noise characteristics. We calculated baroclinic components by subtracting the depth-mean current from each component, combining this with the vertical velocity estimates from the displacement analysis (Fig. 4). The combined ADCP and vertical velocity record were used to estimate the depth-integrated baroclinic kinetic energy,

$$K = \int_{-H}^{0} \left(u'^2 + v'^2 + w^2 \right) dz.$$

These estimates were then scaled by the inverse fraction of depth resolved by the ADCP measurement, to account for the lack of coverage in the near-surface and near-bottom layers. Estimates of available potential energy (APE) were derived using two methods. The "quadratic" method derived from linear internal wave theory [*Scotti et al*., 2006] uses the displacement estimates in the expression $(1/2)\rho_0 N^2 \eta^2$. A more general definition is based on sorting the observed density field into a reference state $(\bar{\rho})$ representing the lowest available potential energy. The "full" APE, calculated using the method of [*Klymak et al.* 2006], is

$$P = \int_{-H}^{0} g\left(\rho - \bar{\rho}\right) z \, dz.$$

In practice, the reference state is calculated by averaging the observed density field by preferentially weighting the upstream density over the rest of the record. The calculations here use a 10-fold weighting advantage applied to the initial CTD profile, relative to the rest of the 160-m isobath timeseries, as a means of defining a background field. Figure 4 shows estimates of baroclinic kinetic energy and potential energy for the 12-hr record at the 160-m isobath. Estimates for kinetic and potential energy are comparable. Moreover, there is not a notable difference between the quadratic and full APE estimates, with each reaching levels of 6.5 kJ/m^2 during the strongest baroclinic activity.

Discussion

We have examined a collection of dissipation measurements across a region of the continental margin of the SCS. The integrated dissipation across our continental shelf section, $\int_{Y_1}^{Y_2}\left(\int_{-H}^{0} \rho\varepsilon \, dz\right)dy$, integrated from the 300- to 40-m isobath, is roughly 3 kW/m. Given the expectation that baroclinic waves drive much of the kinetic energy being dissipated, it is reasonable to ask what level of dissipation is supported by frictional `done by the bottom boundary layer using the standard relation $\rho_0 c_d u^2 |u|$, taking c_d=0.0025 and $u \approx 0.1$ m/s as a (generous) scale for the root-mean-square barotropic tidal current amplitude over the shelfbreak region relevant to our study. The predicted level of frictional dissipation of about 2.5 mW/m^2 is an order of magnitude less than the average dissipation level we observe. This is a strong indictor that the observed dissipation levels derive mostly from the baroclinic energy.

Our observations show waves of near buoyancy frequency, but with ambiguous depression/elevation character. Near-bottom baroclinic activity seems elevation-like, particularly after 1600 UTC. Closer to the surface, there are depression-like anomalies, such as those after 2100 UTC. The complexity of the wave structure is most likely related to the stratification (Fig 2 inset), with the mid-depth buoyancy gradient minimum separating upper and lower stratified layers. For our 160-m isobath record, we can infer wavelengths by scaling the time axis of our record by the mode-1 baroclinic eigenspeed of $c = 0.6$ m/s. This suggests widths of $dx = c \cdot dt \simeq 250$ m for wave in the upper stratification. Taken with the wave displacements from the temperature record, we find

waves with approximate steepness of 1 in 10 (rise over run), indicating significant nonlinearity. Studies by *Klymak and Moum* [2003] and *Scotti et al.* [2006] both describe continental margin environments with energetic nonlinear waves, with comparable amplitudes and aspect ratios to those observed in the current study.

Gawarkiewicz et al. [2004] point out that the depth structure of the buoyancy field during April and May along the northern SCS shelfbreak depends on the state of the transition between the winter and summer monsoon. During ASIAEX in April-May of 2001, the stratification structure was rather shallow, with a buoyancy gradient maximum at 20-m depth. During our study in 2005, winter monsoon conditions lingered into April, and we found buoyancy gradient maxima between 50 and 100-m depth, comparable to the conditions observed in April-May of 2000 by *Gawarkiewicz et al.* Thus, our observations represent a deeper stratification regime of the shelfbreak region than characterized by *Orr and Mignerey* [2003] and *Duda et al.* [2004]. While these authors describe observations of Luzon soliton-like depression waves clearly passing the 160-m isobath in 2001, we saw no such events in 2005. With the deeper stratification, our wave observations were always of the long-train or elevation variety. It is thus likely that the dissipation levels we observed in 2005 are different from those relevant to the shallower stratification regime characterized by the ASIAEX observations.

Our baroclinic energy estimates for the shelfbreak are based on our 12-hr timeseries at the 160-m isobath. This limited record shows maximum energy flux of $F = c \cdot E \cong 8$ kW/m, and a 12-hr mean of 3.8 kW/m. The latter is very close to *Chang et al.* [2006]'s estimate for this region's internal tide energy flux, based on their much longer current meter record. *Chang et al.* [2006] estimate that nonlinear waves comprise 20% of the baroclinic energy flux at the shelfbreak, a much-diminished fraction relative to the nearby Dongsha Plateau. Our results support the finding of *Chang et al.*, that much of the baroclinic energy of the Luzon waves dissipated before reaching the continental shelf off China. This makes the observed dissipation levels all the more impressive, as the trickle of Luzon energy that propagates onto the SCS shelfbreak still drives one of the most dissipative coastal regions of the oceans.

Acknowledgements

I thank J. Wang of National Taiwan University, and the officers and crew of the R/V *OR1* for the opportunity to work with them in the SCS. G. Gawarkiewicz was a primary collaborator in the overall project, and provided many helpful insights into the oceanography of the SCS. I also thank P. Lazarevich and Frank Bahr for their efforts in supporting the measurements. R.-C. Lien, M.-H. Chang, and B. Reeder, provided help in interpreting backscatter and ADCP data. E. Shroyer, J. Klymak, and A. Scotti and provided code for the fully nonlinear APE calculation. This work was supported by the US Office of Naval Research.

References

Chang, M.-H., R.-C. Lien, T. Y. Tang, E. A. D'Asaro, and Y. J. Yang (2006), Energy flux of nonlinear internal waves in northern South China Sea, *Geophys. Res. Letters*, 33, doi:10.1029/2005GL025196.

Duda, T. F., J. F. Lynch, J. D. Irish, R. C. Beardsley, S. R. Ramp, C.-S. Chiu, T.-Y. Tang, and Y.-J. Yang (2004), Internal tide and nonlinear internal wave behavior at the continental slope in the northern South China Sea. *IEEE J. Oceanic Engineering*, 29, 1105-1130.

Gawarkiewicz, G., J. Wang, M. Caruso, S. R. Ramp, K. Brink, and F. Bahr (2004), Shelfbreak circulation and thermohaline structure in the northern South China Sea: Contrasting spring conditions in 2000 and 2001, *IEEE J. Oceanic Eng.*, 29, 1131-1143.

Gregg, M.C. (1999), Uncertainties and limitations in measuring ε and χ. *J. Atmos. Oceanic. Tech.* 16, 1483-1490.

Hsu, M.-K., A. K. Liu, and L. Cheng (2000), A study of internal waves in the China Seas and Yellow Sea using SAR, *Cont. Shelf Res.,* 20, 389-410.

Klymak, J. M, R. Pinkel, C.-T. Liu, A. K. Liu, and L. David (2006), Prototypical solitons in the South China Sea, *Geophys. Res. Lett.*, 33, L11607, doi:10.1029/2006GL025932.

Klymak, J. M., and J. N. Moum (2003), Internal solitary waves of elevation advancing on a shoaling shelf*, Geophys. Res. Lett*., 30, 2045, doi:10.1029/2003GL017706.

Lien, R.-C., T. Y. Tang, M. H. Chang, and E. A. D'Asaro (2005), Energy of nonlinear internal waves in the South China Sea, *Geophys. Res. Lett.*, 32, L05615, doi:10.1029/2004GL022012.

Munk, W., and C. Wunsch (1998), Abyssal recipes II: Energetics of tidal and wind mixing, *Deep-Sea Res*., 45, 1977-2010.

Orr, M. H., and P. C. Mignerey (2003), Nonlinear internal waves in the South China Sea: Observation of the conversion of depression internal waves to elevation internal waves. *J. Geophys. Res.*, 108, 3064. doi:10.1029/2001JC001163.

Osborn, T., (1980), Estimates of the local rate of vertical diffusion from dissipation measurements, *J. Phys. Oceanogr.*, 10, 83-89.

Scotti, A., R. Beardsley, and B. Butman (2006), On the interpretation of energy and energy fluxes of nonlinear internal waves: an example from Massachusetts Bay, *J. Fluid. Mech*., 561, 103-112.

Smith, W. H. F., and D. T. Sandwell, (1997), Global sea floor topography from satellite altimetry and ship depth soundings, *Science*, 277, 1956-1962.

Wolk, F., H. Prandke, and C. Gibson (2004), Turbulence measurements support satellite observations. *Sea Tech*, 45, 47-52.

Yang, Y. J., T. Y. Tang, M. H. Chuang, A. K. Liu, M.-K. Hsu, and S. R. Ramp (2004), Solitons northeast of TungSha Island during the ASIAEX pilot studies, *IEEE J. Oceanic Eng.*, 29, 1182 – 1199.

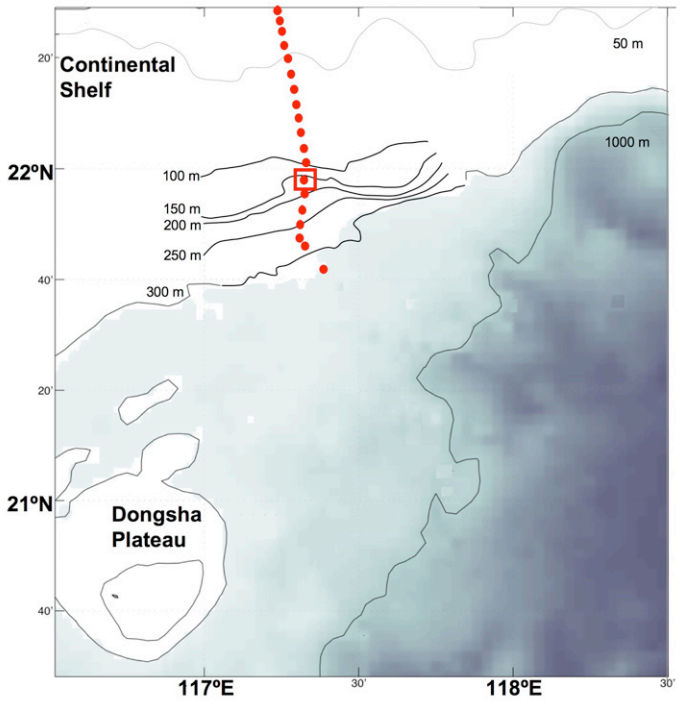

Figure 1

Map showing study region in the South China Sea. Bathymetry from *Smith and Sandwell* [1997] were used for the large-scale bathymetry, while more detailed shiptrack bathymetry collected during ASIAEX was used for the isobaths between 100 and 300 m. Survey section station locations are shown as red dots. The 160-m isobath site is boxed.

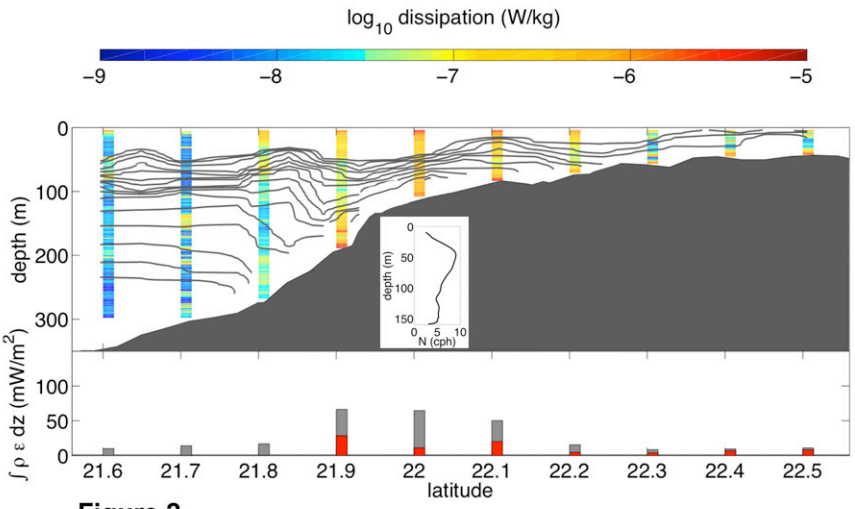

Figure 2

Section spanning the shelfbreak region shown in Figure 1. The temperature field shows a 16-hr synoptic survey that ran from north to south. Contours are shown at 1°C intervals from 14°C to 19°C, and 0.5°C intervals from 19.5°C to 23.5°C. Dissipation rate profiles are shown representing averages from 10 bins equally spaced in latitude along the section. Mean $\log_{10}(\varepsilon)$ profiles are shown for each bin. The depth-integrated mean dissipation levels are shown in the lower panel. The red portion of each bar indicates the contribution of the lower 10-m of the dissipation profile to the integral. The inset panel shows the average buoyancy frequency profile *N(z)* at the 160-m isobath.

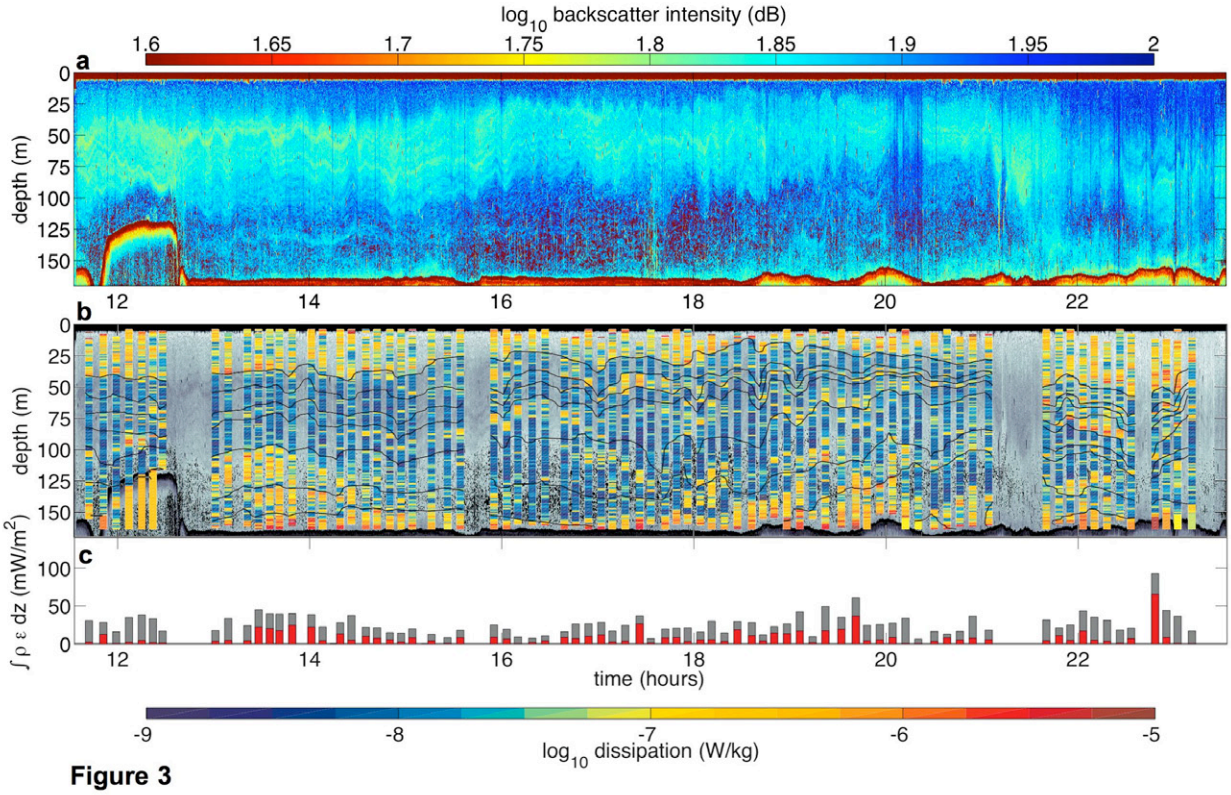

Figure 3

Measurements from the 160-m isobath along the survey section during a continuous 12-hr timeseries where the ship held a constant position. a. Acoustic backscatter data from a 120KHz Simrad EK500 system are shown in upper panel, with a color map corresponding to the upper color bar. b. The same data are shown in the middle panel in grayscale, as a backdrop to the measured dissipation rate profiles, which are shown in color corresponding to the lower color bar. c. Depth-integrated dissipation levels are shown in the lower panel. The red portion of each bar indicates the contribution of the lower 10-m of the dissipation profile to the integral.

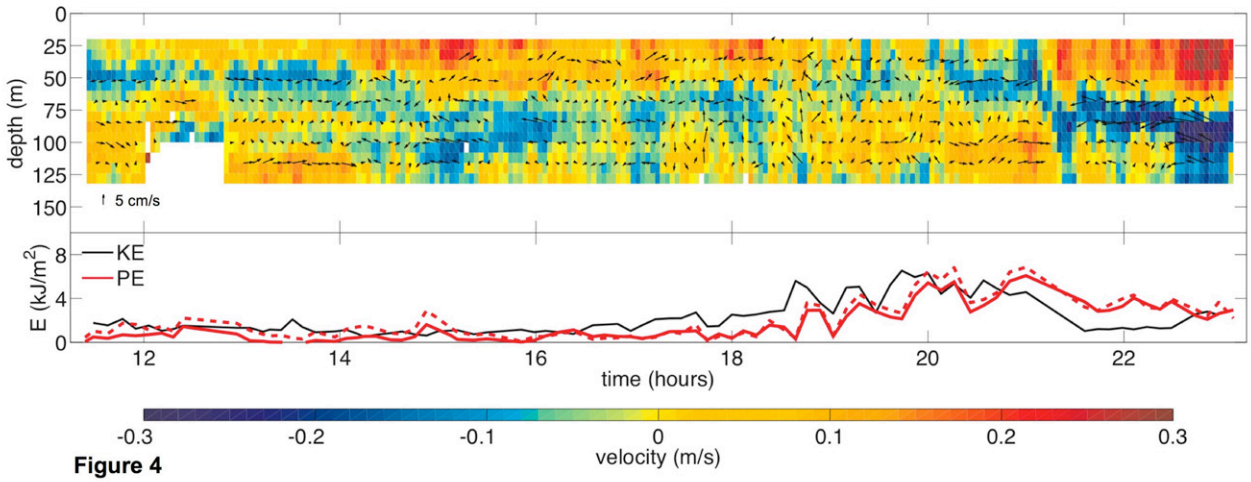

Figure 4

ADCP measured velocity data from the shipboard 150 KHz system are shown in the upper panel for the same 160-m isobath time series shown in Fig. 3. The cross-shelf component of velocity (taken as the northward component - *v*) is shown using the color axis, and the combined cross-shelf (*v*) and vertical velocity components (*w,* estimated from the displacement analysis) are shown as vectors, where the *w*-component has been enhanced relative to the v-component. Maximum vertical velocity magnitudes are ± 0.05 m/s. Energy estimates are shown for both kinetic (black line) and potential (red lines). Potential energy was estimated using both quadratic (dashed red line) and fully nonlinear (solid red line) schemes.